ELSEVIER

Contents lists available at ScienceDirect

Separation and Purification Technology

journal homepage: www.elsevier.com/locate/seppur





Rational design of a small peptidomimetic ligand to capture a viral spike protein

Carlos Filipe Santos Costa ^{a,b}, Iana Lychko ^{a,b}, Carolina Mota Natal ^{a,b}, Arménio Jorge Moura Barbosa ^{a,b,*}, Ana Margarida Gonçalves Carvalho Dias ^{a,b,*}, Ana Cecília Afonso Roque ^{a,b,*}

- ^a Associate Laboratory i4HB Institute for Health and Bioeconomy, Chemistry Department, NOVA School of Science and Technology, Campus Caparica 2829-516 Caparica, Portugal
- b UCIBIO Applied Molecular Biosciences Unit, Department of Chemistry, NOVA School of Science and Technology, NOVA University Lisbon, 2829-516 Caparica, Portugal

ARTICLE INFO

Editor: Cristiana Boi

Keywords: Spike protein Synthetic ligands Affinity chromatography Molecular modelling De novo design

ABSTRACT

The availability of purified antigenic proteins is critical to develop agents to prevent, diagnose, or treat infectious diseases. In this context, antigenic proteins are produced by recombinant expression in host cells and further purified, typically by chromatographic methods. Chromatographic steps that allow the one-step capture of the antigenic protein are important to streamline the purification train. Here, we present the design and development of an adsorbent bearing a synthetic affinity ligand to capture the SARS-CoV-2 spike protein, used as a model antigenic protein. A 120-ligand combinatorial library was designed *in silico* and then synthesised in solid phase, and both were computationally and experimentally screened for binding to the spike protein. One lead ligand was selected for yielding > 95 % binding, and 64–73 % recovery of original strain spike protein, its receptor-binding domain (RBD), and Omicron BA.5 variant spike protein. An enrichment factor of 15 was found when capturing the spike protein from a clarified supernatant sample. Complementary molecular dynamics simulations allowed a better understanding of the interactions between the lead ligand and the spike protein, which mainly consist of hydrophobic interactions, some hydrogen bonds and salt bridges formed with an important ligand carboxyl group. Overall, the methodology is a fast and efficient platform to develop affinity ligands for the purification of antigenic proteins in future pandemics.

1. Introduction

Viral proteins are important antigenic agents with various biotechnological and biopharmaceutical applications [1–3]. For this purpose, there is a high demand for pure antigenic viral proteins to support the development of therapeutic drugs, to improve diagnostic methods, or even to serve as preventive vaccine agents. The SARS-CoV-2 spike protein is a large (ca. 600 kDa [4]) transmembrane trimeric glycoprotein responsible for viral entry and immune evasion, which has been the main target for ligand development [5,6]. However, this protein is constantly mutating with each variant, increasing the risk of antigenic escape [7,8]. The spike protein is typically purified via multiple chromatographic steps. When using tagged spike proteins, stationary phases

are modified with affinity ligands against the respective tags (e.g., histidine tag, Strep-tag, or FLAG M2 tag), which then require additional steps for tag removal. The protein can also be produced without tags, and in this case target-specific steps are used, such as immunoaffinity chromatography, or lectin-chromatography, which rely on expensive and unspecific resins [4,9]. The development of an affinity adsorbent for the fast capture of the untagged target spike protein, can contribute to decrease the number of chromatography steps needed.

Biomimetic ligands are small synthetic ligands designed to mimic the interaction between natural ligands and the target of interest, or *de novo* designed to target unexplored regions of the target. These ligands are inexpensive and fast to develop, easily scalable, and exhibit high chemical stability and resistance to cleaning-in-place (CIP) protocols

https://doi.org/10.1016/j.seppur.2025.132778

Received 30 December 2024; Received in revised form 16 March 2025; Accepted 29 March 2025 Available online 1 April 2025

1383-5866/© 2025 The Author(s). Published by Elsevier B.V. This is an open access article under the CC BY-NC license (http://creativecommons.org/licenses/by-nc/4.0/).

^{*} Corresponding authors at: UCIBIO – Applied Molecular Biosciences Unit, Department of Chemistry, NOVA School of Science and Technology, NOVA University Lisbon, 2829-516 Caparica, Portugal.

E-mail addresses: aj.barbosa@fct.unl.pt (A.J. Moura Barbosa), margarida.dias@fct.unl.pt (A.M. Gonçalves Carvalho Dias), cecilia.roque@fct.unl.pt (A.C. Afonso Roque).

[10]. Different combinatorial chemistry approaches have been used to design and develop such small ligands, namely mix-and-split methods using the triazine scaffold [11], and one-pot reactions using the Petasis and Ugi reactions [10,12]. Such ligands can be further coupled to a variety of purification matrices, from common chromatographic adsorbents [10], to magnetic beads [13], monoliths [14], and membranes [15], and used to purify various biological targets with different complexity, including peptide tags [16], proteins [10], and viral particles [17]. Several ligands targeting the SARS-CoV-2 spike protein have been reported, the majority being peptides and proteins. These ligands were developed using computational design, protein/peptide discovery and evolution, as well as combinatorial methods. This topic has been recently thoroughly reviewed [18]. Despite the success of these peptide-based ligands, there is no report of small synthetic peptidomimetic ligands designed to target the SARS-CoV-2 spike protein.

Here, we describe the design and selection of a peptidomimetic ligand binding to the SARS-CoV-2 spike protein, used as a model antigenic protein. The ligand was selected from a rationally designed combinatorial library of putative ligands mimicking the interactions established between the spike protein and known ligands [18]. The overall development process (Fig. 1) allowed the fast development of a ligand binding to a viral surface antigenic protein, successfully employed as an adsorbent for target capture and recovery.

2. Materials and methods

2.1. Biological materials

The recombinant original strain spike protein was kindly provided by the Institute of Bioprocess Science and Engineering of the University of Natural Resources and Life Sciences (BOKU), Vienna, Austria, via the BOKU-COVID19 portal from the WWTF COVID-19 Rapid Response Call programme (UniProt PODTC2), as well as by the Instituto de Biologia Experimental e Tecnológica (iBET), Lisbon, Portugal (GenBank

QJE37812.1 [19], which has 99.5 % identity to UniProt PODTC2, as calculated with Expasy SIM; trimeric MW ca. 600 kDa [4]). Expi293F clarified supernatant of the same spike protein production was also kindly provided by iBET [4]. Recombinant original strain spike protein receptor-binding domain (RBD; purity > 95 %, as determined by sodium dodecyl sulphate–polyacrylamide gel electrophoresis (SDS-PAGE); MW ca. 34 kDa) and recombinant Omicron BA.5 variant spike protein (purity > 90 %, as determined by SDS-PAGE and SEC-HPLC; monomeric MW ca. 150 kDa) were purchased from Sino Biological (40592-V08B and 40589-V08H33, respectively).

2.2. Rational design and virtual screening of the combinatorial library

Molecular visualisation software PyMOL 2.4.1 [20] was used to analyse the structures of spike protein in complex with a ligand from the Protein Data Bank (PDB) [21], searching in particular for ligand residues or clusters thereof establishing important interactions near spike protein interaction hot spots, as identified in [18] (PDB 7K9Z, 7DK4, 7DK5, 7DK6, 7DK7, 7DCC, 7DCX, 7DD2, 7DD8, 6WPS, 6WPT, 7KKL, 7JZL, 7JZU, 7JZM and 7JZN). Considering that the scaffold of Petasis-Ugi ligands allows up to four different functional groups, these clusters were divided into groups of up to four residues. The free online chemical database ChemSpider [22] was then used to search for Petasis-Ugi reagents (boronic acids, amines, aldehydes, and isocyanides) with similar moieties to the functional groups of these ligand residues. Due to the relative scarcity and toxicity of isocyanides, only isopropyl isocyanate was used and maintained constant. Three boronic acids were selected (4aminocarbonylphenylboronic acid, 3-aminophenylboronic acid and 1Hindene-2-boronic acid), eight amines (ethanolamine, 1-aminopropan-2ol, β-alanine, 1.3-diaminopropane, agmatine, 1-pyrrolidineethanamine, histamine and 4-hydroxybenzylamine), and five aldehydes (isovaleraldehyde, 3-(methylthio)propionaldehyde, 4-formylbenzoic acid, phenylacetaldehyde and indole-2-carboxaldehyde) to integrate the combinatorial library, resulting in 120 different combinations (i.e., 120

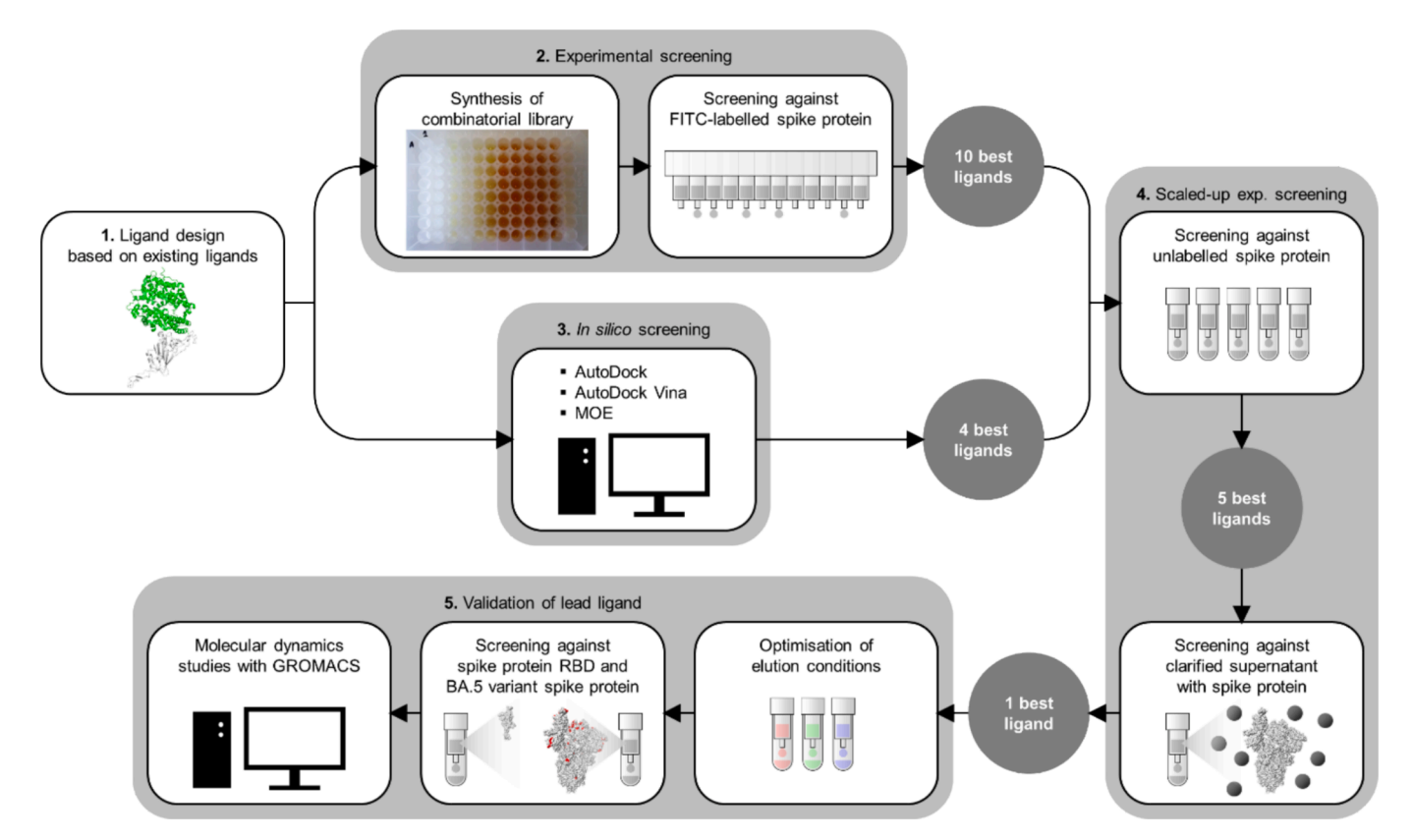


Fig. 1. Schematic representation of the development process for the novel Petasis-Ugi affinity ligands targeting the SARS-CoV-2 spike protein.

different ligands).

For the virtual screening, blind dockings of the combinatorial library against the spike protein RBD structure were performed with AutoDock 4.2.6 and AutoDock Vina 1.2.0 [23,24] using PyRx 0.8 [25], and with Molecular Operating Environment (MOE) 2022.02 [26] against the spike protein RBD (residues 319–541), for not only it is unglycosylated, but also the most common target for binding to ligands. The spike protein structure was retrieved from the PDB with the highest completeness and resolution available at the time of the experiment (PDB 7DWZ). One of the RBDs was isolated from the whole structure using PyMOL before adding charges with UCSF Chimera 1.15 [27] using the AM1-BCC method.

To elaborate the 120-ligand combinatorial library, the chemical structures of the backbone and functional groups were created in ChemDraw 20.1 [28] and subsequently imported into DataWarrior 5.5.0 [29], where the library was generated. The library was exported into a single SDF file, and then the energies of the ligands were minimised with Open Babel 3.1.1 [30]. Ligand isoelectric points and protonation states were estimated with MarvinSketch 19.12 [31].

The protein and ligand files were converted to the PDBQT format for AutoDock and AutoDock Vina with Open Babel. In AutoDock, the minimum number of energy evaluations was set to 25 M and the number of runs per ligand to 10. In AutoDock Vina, the exhaustiveness was left at default 8. In MOE, the rigid receptor refinement method and London dG scoring function were used. All remaining parameters not mentioned from either of the three docking tools were left at default settings. All protein–ligand complex structures were visualised with PyMOL.

2.3. Solid-phase synthesis of the combinatorial library

Sepharose CL-6B was aminated in-house following a procedure described in [12] and detailed in Supporting Information (SI). The synthesis of the combinatorial library in 96-well microplates (Captiva 96-well 20 μm filter plates) was performed as detailed in SI and as previously published [10]. Briefly, 0.25 g of agarose beads were added to each well. The ligand synthesis started with a Petasis reaction in which the boronic acid moiety was introduced, followed by the Ugi reaction in which the amine, aldehyde and isocyanide moieties were introduced (Fig. 2 and Fig. S1 in SI).

2.4. Combinatorial library screening and ligand assessment

The combinatorial library was firstly screened for spike protein binders by using a fluorescently labelled spike protein. The recombinant original strain whole spike protein was labelled with fluorescein isothiocyanate (FITC), following the supplier's protocol and detailed in SI. The *in situ* screening of the 120-membered ligand library was made directly on the 96-well microplates and as previously described [10]. The binding buffer was designed based on standard conditions typically used for the purification of virus-like particles (VLPs) [32] (0.01 M HEPES, 0.15 M NaCl, pH 7.4). After an initial equilibration step with the binding buffer, each well containing 0.25 g resin (moist gel) was loaded with 250 μ L of a fluorescently labelled spike protein loading solution (0.98 \pm 0.05 μ g/mL). The beads were then washed with the sample volume (250 μ L) of binding buffer and all samples collected. The amount of FITC-labeled spike protein was quantified and the percentage of binding estimated (details in SI).

After this initial screening, a second screening assay was performed with the top 14 adsorbents selected (10 from the FITC-labelled screening plus 4 from the virtual screening). Here, spin columns were used (900 μL Pierce spin columns from Thermo Fisher Scientific). In this assay, 70 mg of each resin (moist gel) were packed in the spin columns, equilibrated with binding buffer, then loaded with 140 μL of the recombinant original strain whole spike protein (27.5 \pm 0.6 $\mu g/mL$), incubated for 1 h at room temperature with rotational agitation at 20 rpm, and then washed with the sample volume (i.e., 140 μL) of binding buffer. Between each

step, a quick centrifugation step was added (1200 rpm for 30 s). After the second screening assay, a set of 5 ligands were chosen to carry out the studies. These 5 adsorbents (70 mg of moist gel) were packed in spin columns, and the same method was applied. However, in these tests, the loading was a clarified supernatant containing the recombinant original strain whole spike protein (550.2 \pm 35.8 µg/mL total protein of clarified supernatant containing 19 % recombinant spike protein, as determined by SDS-PAGE densitometry). While the binding buffer was maintained constant, two elution buffers were sequentially tested (0.01 M HEPES, 1 M NaCl, pH 7.4 and 0.1 M glycine, pH 2.5). For this, n x 140 µL of each buffer were used, and the first column volume was left incubating for 15 min before spinning. The collected samples were quantified by the Micro BCA method.

Finally, the lead adsorbent selected was packed (0.75 g moist gel) in gravitational columns (Bond Elut 3 mL columns, Agilent), Firstly, the elution conditions were optimised. For this, 750 µL of the pure recombinant original strain whole spike protein were loaded (17.05 \pm 0.36 $\mu g/mL$). After washing with binding buffer (750 μL at a time, until the absorbance at 280 nm was negligible), bound protein was recovered by different elution buffers (listed in Table S4 in SI; 750 µL at a time, until the absorbance at 280 nm was negligible). All elution buffers were tested on separate columns. After selecting the best elution buffer, the columns were tested for binding to and eluting spike protein from the clarified supernatant, and then tested for binding and recovery of distinct spike protein fragments and variants, namely recombinant original strain spike protein receptor-binding domain (RBD), and recombinant Omicron BA.5 variant spike protein from Sino Biological. The collected samples were quantified by the Micro BCA, or SDS-PAGE densitometry methods, indicated in the results section. Further analysis were conducted to assess adsorbent re-use and dynamic binding capacity. Purified spike protein obtained in the elution fractions with the lead ligand was characterized by Western-blot (anti-His antibody), ATR-FTIR, ELISA (for binding to ACE) and DNA clearance estimated. These details can be found in SI.

2.5. Molecular modelling of spike protein and lead ligand

Molecular dynamics (MD) of the RBD in complex with the lead ligand B1A3AL4 were performed with GROMACS 2024.1 [33] on Ubuntu 22.04, in an Intel Core i7 14700KF, an NVIDIA GeForce RTX 4080 SUPER and 64 GB of random-access memory (RAM). Both the protein and ligand structures selected from the docking results were protonated to the appropriate pH (7.4 for binding conditions and 2.5 for elution conditions) with Open Babel. For the protein, an Assisted Model Building with Energy Refinement (AMBER) force field was used, AMBER99SB-ILDN [34]. Ligand topologies were generated with ACPYPE 2023.10.27 [35], a Python interface for Antechamber [36,37], which is an automated parameterisation tool based on the General AMBER Force Field (GAFF) [36,37]. The boxes generated were cubic, with 1.2 nm padding.

The protein–ligand complex structures were first subjected to an energy minimisation based on steepest descent with a 0.01 nm step size until maximum force was $<1000~\rm kJ\cdot mol^{-1}\cdot nm^{-1}$, followed by another using conjugate gradient with a 0.01 nm step size until maximum force was $<400~\rm kJ\cdot mol^{-1}\cdot nm^{-1}$. Next, the systems were heated to 298 K for 0.5 ns using the Berendsen thermostat before equilibrating them with constant temperature and pressure for 0.5 ns using the V-rescale thermostat and the C-rescale barostat. Both equilibrations were performed with 0.002 ps time steps, particle mesh Ewals (PME) electrostatics, and cut-off van der Waals method, each with a 1 nm cut-off. Finally, the production runs were performed in triplicates for 100 ns each, using the V-rescale thermostat and the C-rescale barostat, and 1 nm cut-offs for non-bonded interactions.

Free energy calculations were performed with gmx_MMPBSA 1.6.3 [38,39], in which the Poisson-Boltzmann equation was applied throughout the 100 ns of the production runs. The results were

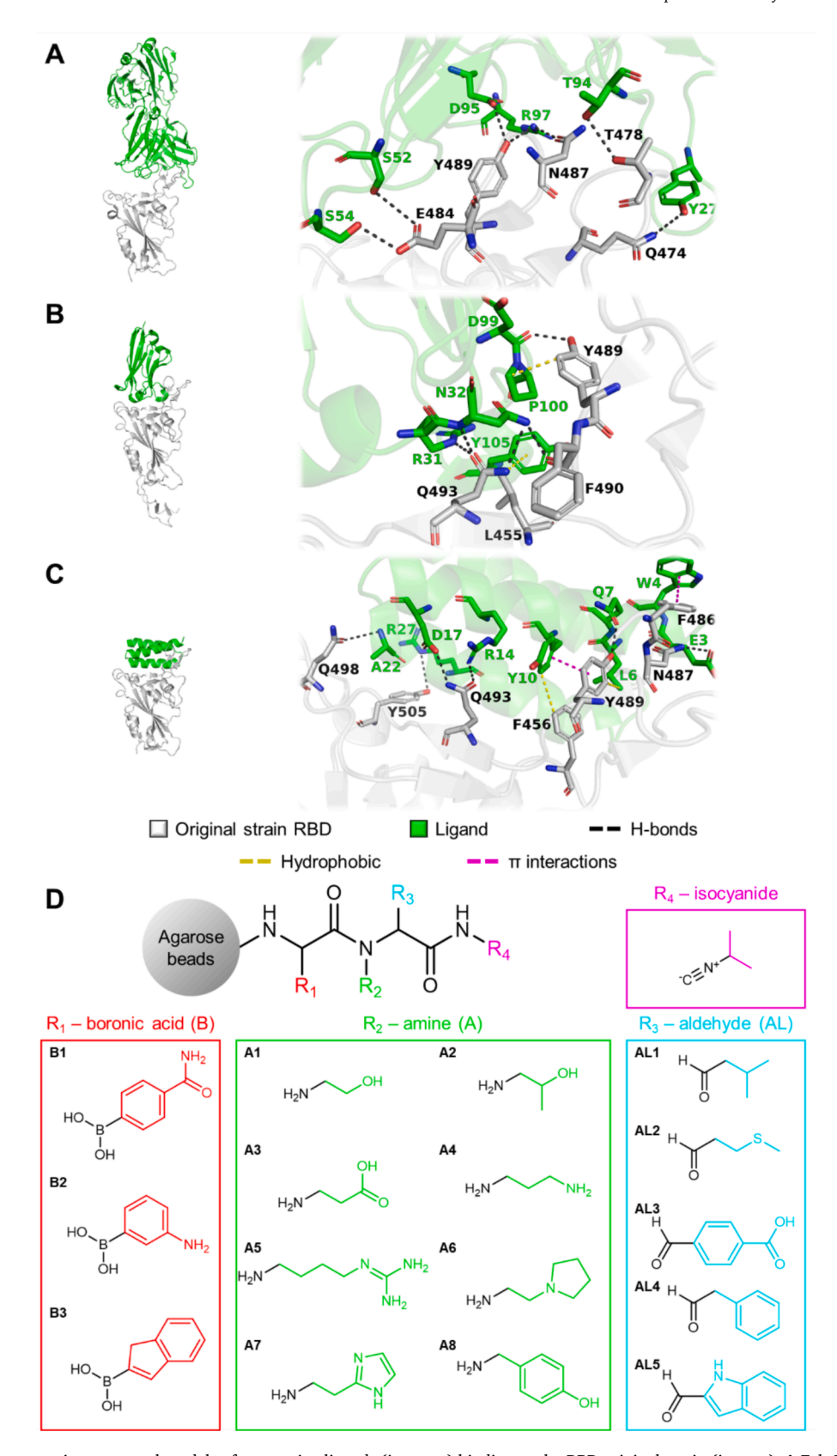


Fig. 2. Examples of representative structural models of non-native ligands (in green) binding to the RBD original strain (in grey): A Fab 298, B VHH mNb6, and C peptide scaffold LCB1. D Petasis-Ugi reagents selected for the combinatorial library. The code henceforth used for each compound is next to its structure.

visualised with PyMOL [20] and the data treated using GROMACS tools (gmx energy, gmx rms, gmx rmsf and gmx distance) and OriginPro 2021 [40].

3. Results and discussion

3.1. Rational design of a combinatorial library of ligands

There are a number of ligands targeting the SARS-CoV-2 spike protein [18]. To rationally design the ligand library, we selected a small set of these known ligands. We considered those displaying the lowest equilibrium dissociation constants (KD) towards the spike proteins, as reported in the literature. In more detail, a cut-off of 0.001 nM was defined for the fragment antigen-binding (Fab) and single-domain antibody (VHH) fragments. To have at least one ligand from each family, the cut-off for the *de novo* designed peptide scaffolds was of 0.1 nM. Ultimately, nine ligands were selected: hACE2, five Fabs, one VHH fragment, and two peptide scaffolds (Table S1). The structures of these nine ligands in complex with the spike protein were analysed using PyMOL [20] (Fig. 2A-C). As the Petasis-Ugi scaffold allows for up to four different functional groups (Fig. 2D), clusters of up to the same number of ligand residues interacting with known spike protein hot spots were noted (Table S2). The number of occurrences of each ligand residue was also taken into consideration (Fig. S2).

With this information, a search was conducted using the online database ChemSpider [22] for compounds containing one of the functional groups involved in the Petasis or Ugi reactions, namely boronic acids, amines, aldehydes or isocyanides, as well as one moiety similar to the functional groups of the most prevalent amino acids listed above. Both availability and risk of cross-reactivity were considered in the selection of the compounds. In the end, three boronic acids, eight amines, five aldehydes and one isocyanide were selected (Fig. 2D), resulting in a combinatorial library of 120 different ligands.

3.2. Screening of synthetic ligand combinatorial library

The 120-ligand combinatorial library was screened for binding spike protein through experimental and computational methods.

For the experimental screening, the 120-membered ligand library was synthetised and screened on chromatographic beads, and each ligand tested for binding to FITC-labelled spike protein. A cut-off of 80% binding allowed to select the top 10 ligands to be further analysed (Fig. 3A).

The 120-ligand combinatorial library of ligands was also virtually screened for binding to the original strain spike protein RBD using a blind docking approach. For this purpose, three different docking software were used, namely AutoDock, AutoDock Vina and MOE, to minimise bias. The results from each of the three software were ordered by binding energy before visually analysing the structures of the 30 best RBD-ligand complexes from each docking run. The complexes in which the ligand had its support-binding terminal towards the protein were excluded, since it would be inaccessible when in the solid matrix. Overall, there were not many similarities in results observed for each of the three software, which could be attributed to the different placement algorithms and scoring functions. Nevertheless, four ligands were found amongst the top 10 molecules with the lowest binding energy of at least two distinct docking software (Fig. 3B-D and Fig. S3), which were included in the top 10 selected from the experimental screening. These four ligands were mutually similar only in that they all possessed three hydrophobic groups each. The docking sites were slightly different for each of these four ligands and across the three simulations, varying between the hACE2 binding site on the RBD and its side that faces the solvent when in the spike protein is in the "down" conformation.

3.3. Lead ligand selection

Considering both the experimental and virtual screening results, a set of 14 putative lead ligands were selected to proceed with the studies (Fig. S4).

To confirm the performance of the ligands, these were packed into columns and tested for binding unlabelled pure spike protein. Of the 14 lead ligands, seven yielded at least 50 % binding (Fig. 4A). The best ligand for spike protein capture was B1A3AL4, with 91 \pm 9 % binding. Since B1A4AL4 possessed an almost identical chemical structure to B1A3AL4, except for one charged functional group (negatively charged in B1A3AL4 and positively charged in B1A4AL4), it could be inferred that a negatively-charged functional group was more advantageous for binding to the spike protein, given the considerable disparity between the binding of these two ligands (Fig. S4). Thus, B1A4AL4 was excluded from the selected lead ligands for further assays. Likewise, B3A3AL5 and

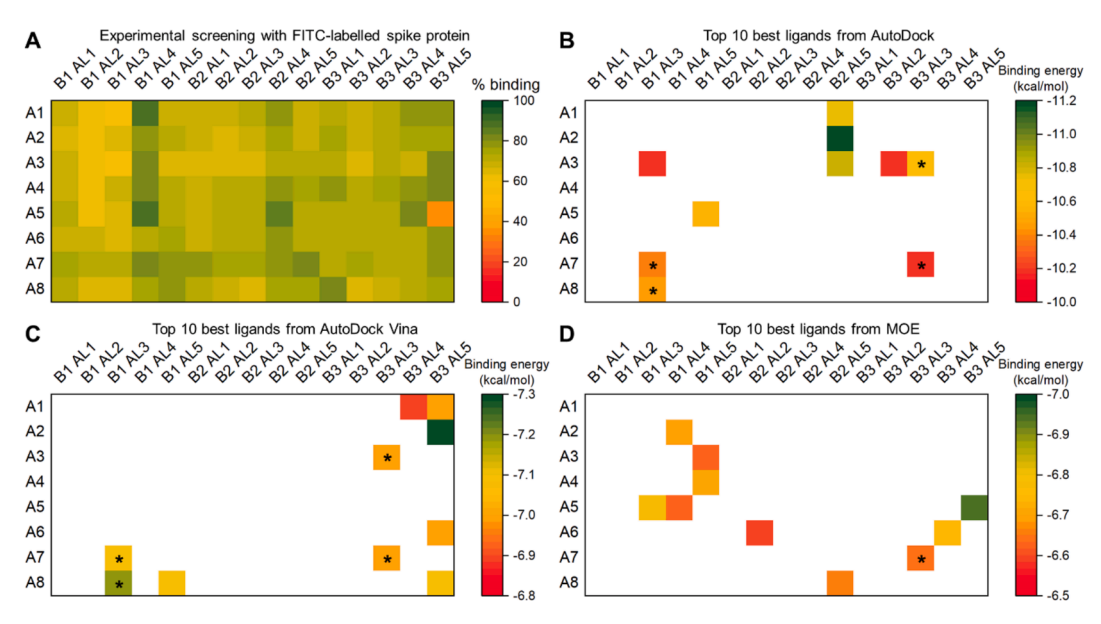


Fig. 3. Screening results from the 120-ligand combinatorial library: **A** experimentally, against FITC-labelled recombinant original strain spike protein, where a cutoff of 80% binding allowed to select 10 lead ligands, and *in silico*, using **B** AutoDock, **C** AutoDock Vina, and **D** MOE. Poor binders in red, mild in yellow and top in green. The four ligands occurring amongst the top 10 best from at least two docking software are highlighted with an asterisk.

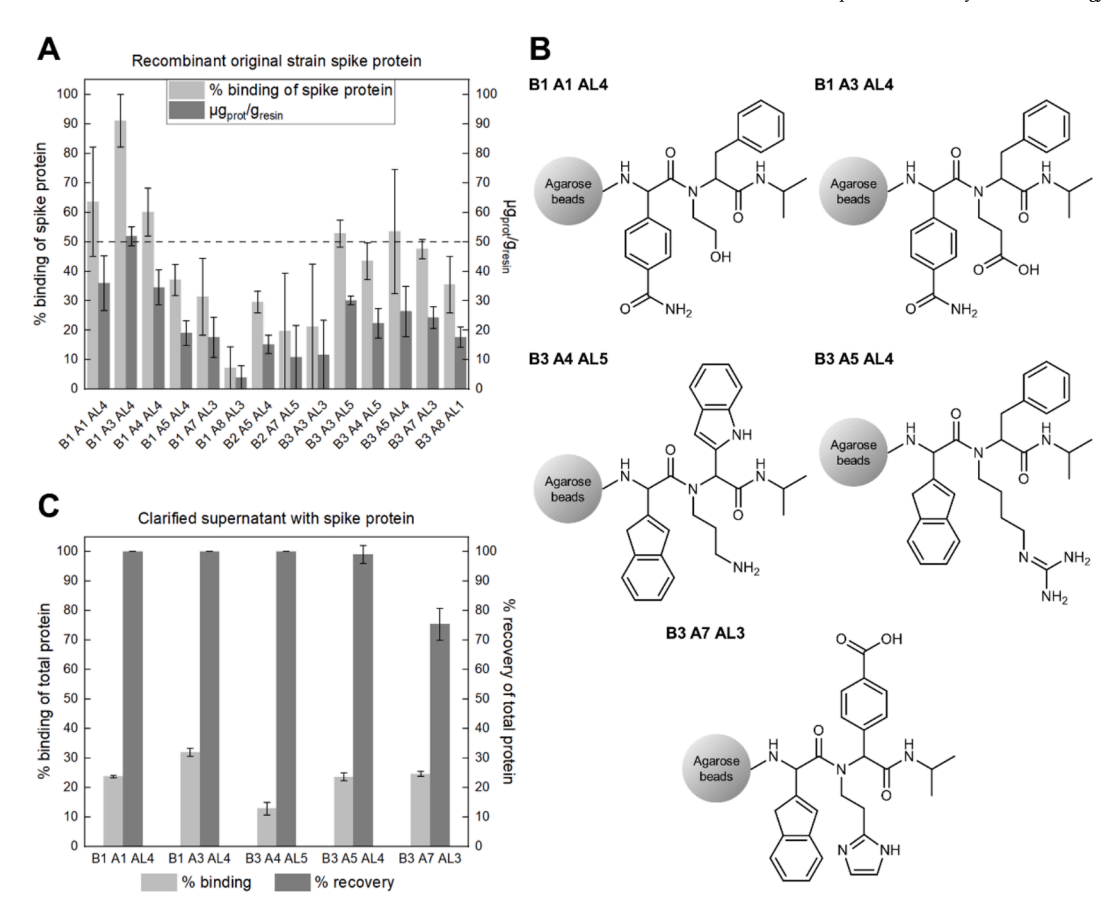


Fig. 4. A Results from the experimental screening of the 14 lead ligands against pure unlabelled recombinant original strain spike protein. The cut-off of 50% binding is shown as a dashed line. B Top five lead ligands yielding at least 50% binding against pure unlabelled recombinant original strain spike protein. C Results from the experimental screening of the five lead ligands against clarified supernatant with recombinant original strain spike protein, calculated from the total amount of protein.

B3A4AL5 differed only in one charged functional group but presented similar binding to the target. To increase structural diversity in the top ligands, B3A4AL5 was selected to proceed due to the positively charged group. In the end, five lead ligands were selected for further assays (Fig. 4B).

These five ligands were then screened against a clarified supernatant containing recombinant spike protein to assess selectivity in binding. For this assay, recovery was also considered to evaluate the performance of each ligand (Fig. 4C). As such, preliminary elution conditions were designed based on the ligands' chemical structures and possible interactions with the target. Except for B1A1AL4, all the other lead ligands possessed at least one charged functional group, with B1A3AL4 displaying a negatively charged carboxylic group, B3A4AL5 and B3A5AL4 a positively charged amine and polyamine, respectively, and B3A7AL3 behaving as a zwitterion, exhibiting both a negatively charged carboxylic acid and a positively charged imidazole group. The isoelectric points and protonation states of each lead ligand were estimated with MarvinSketch [31] (Table S3).

A high salt concentration elution buffer was used to disrupt the electrostatic interactions between the ligands and the spike protein. Specifically, a higher salt concentration version of the binding buffer was chosen (0.01 M HEPES, 1 M NaCl, pH 7.4). However, the amount of protein recovered was negligible. Changing the pH can affect the ionisation state of residues, therefore a low pH elution buffer typically used in affinity chromatography was sequentially employed (0.1 M glycine, pH 2.5) [41]. The amount of protein recovered was considered as the sum of the eluates with both elution buffers.

The adsorbent bearing the ligand B1A3AL4 yielded the highest % binding of total protein (31.9 \pm 1.3 %) and, along with B1A1AL4 and

B3A4AL5, a high % recovery of total protein (100 %). These results corroborated those from the previous screening assay, highlighting B1A3AL4 as the best-performing ligand.

3.4. Optimisation of chromatographic conditions for the lead ligand

The lead adsorbent modified with the ligand B1A3AL4 was further optimised for binding and elution of the spike protein. Firstly, the chromatographic conditions for capture and recovery of pure recombinant original strain spike protein were scaled up, by using 0.75 g of moist agarose and sample volumes of 750 μL . Whilst the binding conditions were maintained constant, a set of elution buffers was tested. The interactions established between B1A3AL4 and the spike protein RBD resulting from the docking studies were analysed, to guide the selection of elution buffers.

The best results from each docking run placed the ligand in different sites of the RBD target, with AutoDock and MOE predicting the closest binding sites (on the lateral of the RBD), whilst AutoDock Vina placed the ligand on the receptor-binding motif (RBM). Despite the different binding sites, there were similarities on the types of interactions observed, namely the carboxylic acid of B1A3AL4 forming important hydrogen bonds in all three docking results, or its amide also establishing hydrogen bonds in AutoDock Vina and MOE. The two phenyl groups of the ligand formed hydrophobic interactions in AutoDock and π - π stackings in AutoDock Vina, yet only one salt bridge was found involving the carboxylic acid moiety in MOE (Fig. 5A).

Overall, it was evident that ideal elution conditions should tackle primarily hydrogen bonds and interactions involving hydrophobic residues. As such, 12 additional elution buffers were designed (Table S4)

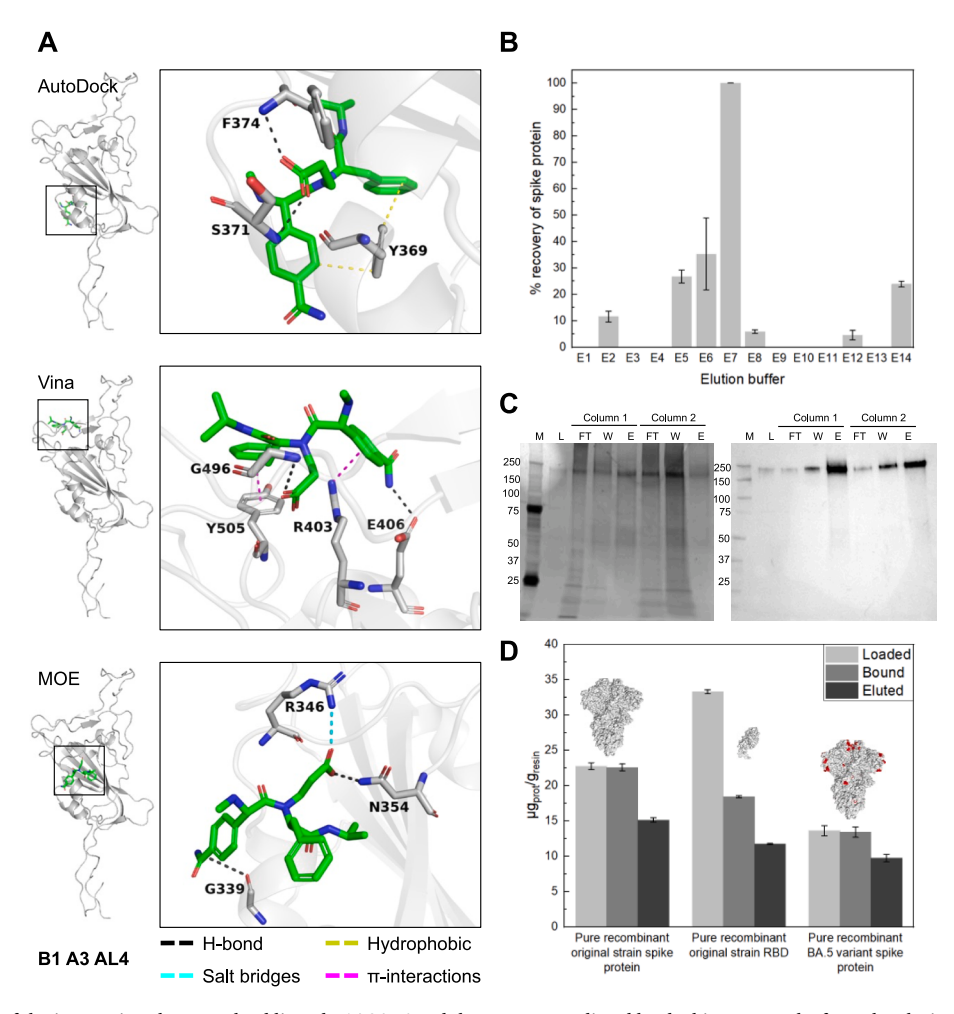


Fig. 5. A Visual analysis of the interactions between lead ligand B1A3AL4 and the RBD, as predicted by docking. B Results from the elution assay of B1A3AL4 against pure recombinant original strain spike protein. C Silver-stained SDS-PAGE of samples, and corresponding Western blot, from screening of B1A3AL4 against clarified supernatant, normalised by volume. M is the marker (NZYColour Protein Marker II); L the loading solution; FT the flow-through; W the washes; and E the eluates. The bands corresponding to the spike protein are in line with the arrow. D Results from the experimental screening of lead ligand B1A3AL4 against pure samples of recombinant original strain spike protein, RBD and BA.5 variant spike protein, represented as μg of protein per g of resin.

and tested with pure recombinant spike protein (Fig. 5B), which combined ionic strength with pH effect and even some competitors or denaturing agents. Our group has used a similar approach in other works [11] in which it was required versatile and more complex elution buffers. Arginine was chosen due to its versatility as a competitor in both ion-exchange and hydrophobic interaction chromatography [42], since it is a zwitterion and thus can bind to either charged residues, plus its guanidinium group can bind to hydrophobic groups [43]. Imidazole was also tested, which acts as a competitive agent for histidine residues on the target protein. In some of the buffers, in which caprylic acid was used, the pH was slightly increased from 6.0 to 7.0, as it began precipitating, since its solubility decreases with low pH [44].

The combination of arginine with NaCl were very efficient in eluting the spike protein bound to B1A3AL4, except for buffer E10, which also contained sodium citrate. This is explained by the fact that arginine, as a positively charged residue, reduces the binding free energy between the protein and the ligand, whilst the negatively charged citrate increases it [45]. Buffer E7, which included the non-ionic surfactant Tween 20, yielded the highest % recovery of pure recombinant spike protein (100 %) and, therefore, was selected as the best elution buffer.

Buffer E7 was used in a repetition of the experimental screening of B1A3AL4 against clarified supernatant containing recombinantly produced original strain spike protein. Due to the complexity of the loading solution, SDS-PAGE densitometry was employed, with all samples normalised by volume (Fig. 5C). The spike protein band (ca. 200 kDa [4])

was not detected in the flow-through or washes lanes, indicating 100 % binding. The % recovery was calculated as 45.5 ± 11.7 %, thus the final enrichment factor was determined as 14.6. To compare the results yielded by the Micro BCA and SDS-PAGE densitometry quantification methods, the latter was used to quantify the samples from the previous experimental screening of B1A3AL4 against pure recombinant spike protein (Fig. 5D and Fig. S5A). Once again, no spike protein bands were found in the flow-through or washes lanes, thus the % binding was assumed as 100 %, which agreed with the 91.0 \pm 9.0 % binding determined by Micro BCA, whilst the % recovery was estimated as 67.0 \pm 2.5 %. We preliminary assessed the presence of DNA in the samples, which was only detectable in the loading and flow-through samples (Table S5). The presence of DNA and HCP deserve deep analysis in the future.

Considering that the docking was performed against just the spike protein RBD due to the high computational requirements and time constrains needed for the whole protein, an experimental screening was also performed with B1A3AL4 against a $33.3\pm0.3~\mu\text{g/mL}$ RBD loading solution, using similar conditions as in the previous assays (Fig. 5D). Quantification was made with Micro BCA, and the % binding and % recovery were calculated as 55.3 ± 4.0 % and 63.6 ± 6.0 %, respectively. The low % binding could be explained by the larger amount of protein in the loading solution. As SARS-CoV-2 underwent several mutations throughout the pandemic, it made sense to test if B1A3AL4 would maintain its performance against a variant spike protein. For this purpose, another experimental screening was performed against a 13.6

 \pm 0.7 µg/mL Omicron BA.5 variant spike protein loading solution, which was the predominant strain at the time of the experiment (Fig. 5D). Micro BCA was used to quantify the samples, except the eluates, which presented interference by the elution buffer even after being dialysed. The % binding was calculated as 98.5 ± 1.2 %, which was ideal and very similar to that obtained for the original strain spike protein. SDS-PAGE densitometry was subsequently employed to quantify all samples (Fig. S5B), with no spike protein bands found on the flowthrough or washes lanes, therefore assuming a % binding of 100 %, and a % recovery of 72.6 \pm 12.2 %. The differences observed in the % binding between full spike proteins and the RBD were most likely related to the binding capacity of the adsorbent, and to stereochemical and multivalency effects when the full trimeric spike protein was used.

We further assessed the structure and activity of the eluted original strain spike protein purified from the clarified supernatant (Fig. 5C). The structure was verified by ATR-FTIR (due to the very low amounts of protein available), whilst the activity against hACE2 was verified by ELISA. The structural analysis by ATR-FTIR revealed similarities between the spike protein before and after purification (Fig. S6 and Table S6). Moreover, the overall secondary structure composition aligned with previously reported data in the literature [46], confirming that the protein maintained its structural integrity. The analysis identified the presence of β -sheets (43.5–48.7 %), α -helices (32.1–44.5 %), β -turns (4.8–5.1 %), and random coils (1.5–19.4 %). The ELISA assay confirmed that the spike protein purified using the B1A3L4 ligand remained active and successfully bound to recombinant hACE2 (Fig. S7). Its activity was comparable to the active control, indicating that the purification method preserved the protein's functional integrity. These findings validate both the specific interaction between the spike protein and hACE2, and the effectiveness of the purification approach.

The number of successive cycles after CIP and the dynamic binding capacity were also assessed for the lead adsorbent. The reusability of the adsorbent was tested in three consecutive purification cycles with spike protein added to spent HEK cell culture media with a CIP step between each run. The performance of the B1A3AL4 adsorbent was not affected by the CIP, as the adsorbent bound and eluted the same amount of protein (Fig. S8 and Table S7). To assess the dynamic binding capacity (DBC_{10%}) of B1A3AL4, a breakthrough curve was performed with RBD (Fig. S9), resulting in 30 µg of RBD per g of adsorbent.

3.5. Understanding interactions of lead ligand with the target

To assess the interactions between the lead ligand B1A3AL4 and the spike protein RBD, MD simulations were performed on the protein–ligand complex structures resulting from the dockings.

Initially, a single 100 ns MD run was performed for the three ligand positions predicted by each of the three docking software in pH binding conditions (pH 7.4), each with a different predicted binding site. In both the complexes predicted by AutoDock and AutoDock Vina, the ligand unbound at approximately 60 and 70 ns, respectively, whereas the one from MOE remained bound (Fig. S10A), therefore the ligand position predicted by MOE was selected and triplicate runs were performed, all of which stayed bound as well (Fig. S10B).

The energy, temperature and pressure plots during the equilibration and production runs for the RBD-lead ligand B1A3AL4 complex structures predicted by each docking software used can be seen in Figs. S11-18. From these results, it was possible to infer no problems occurred during the MD.

The protein–ligand interactions over time were visualised in PyMOL (Fig. 6 and Figs. S21 and S22). The binding pocket on the RBD was slightly below the hACE2 binding site, but nevertheless in an easily accessible region of the RBD, even in its "down" conformation [18]. The ligand terminal facing the agarose matrix remained always fully accessible, and the starting position involved an important salt bridge between the ligand carboxylic acid and the RBD R346 side chain, a

hydrogen bond between the ligand amide and the RBD N343 side chain, and a hydrophobic interaction between the ligand isopropyl group and the RBD V341 side chain (Fig. 6 and Figs. S21 and S22).

In the first run, there were no noteworthy conformational changes in either the RBD or the ligand, as corroborated by the constant short distance between the ligand and the initial binding pocket (Fig. S10). The ligand carboxylic acid and amide showed a very dynamic behaviour, the former alternating between a salt bridge with the RBD R346 side chain and a hydrogen bond with the RBD T345 side chain, and the latter between a hydrogen bond with the RBD N343 side chain and another with the RBD T345 side chain, the latter interaction being easily displaced by the ligand carboxylic acid forming a hydrogen bond with the RBD T345 side chain. The ligand isopropyl group alternated between a hydrophobic interaction with the RBD V341 side chain and another with the RBD F347 side chain. At 11 ns, the ligand flipped in a way that its previously unbound phenyl group established hydrophobic interactions with the RBD A344, F347 and A348 side chains, whilst the ligand carboxylic acid formed a salt bridge with the RBD K356 side chain, but otherwise it remained within the binding pocket (Fig. 6).

Interestingly, in the second run, there was a noticeable conformational change in the RBD at about 40 ns, which coincided with the ligand distancing itself slightly from the initial binding pocket. This could be explained by the RBD changing its conformation to accommodate the ligand. The ligand carboxylic acid exhibited a very dynamic behaviour once again, alternating between a salt bridge with the RBD R346 side chain and a hydrogen bond with either the RBD F347, or A348 backbone amines. The ligand amide also alternated between a hydrogen bond with the RBD N343 side chain and another with the RBD E340 side chain, and later between the RBD N354 and K356 side chains, which caused its isopropyl group to unbind and the ligand to flip, binding slightly outside the pocket with its carboxylic acid forming a salt bridge with the RBD R509 side chain (Fig. S21).

Finally, in the third run, only the ligand underwent a slight conformational change at approximately 40 ns, which was also when its distance to the initial binding pocket increased, however without detaching from the RBD. The ligand carboxylic acid alternated between a salt bridge with the RBD R346 side chain and another with the RBD K356 side chain, until the ligand flipped and its phenyl group formed a cation- π interaction with the RBD R346 side chain. At 45 ns, the ligand deviated slightly from the pocket, establishing multiple weak backbone interactions briefly before settling with a cation- π interaction between its phenyl group and the RBD R466 side chain, whilst its amide formed hydrogen bonds with the RBD R355 and Y396 side chains (Fig. S22).

In summary, it was evident the B1A3AL4 carboxylic acid was its most interactive group, being involved in some of the most important interactions with RBD residues T345, R346, F347, A348, K356 and R509. Meanwhile, its amide also established some important bonds with RBD E340, N343, T345, N354 and K356, whilst its isopropyl and phenyl groups were only involved in weak hydrophobic interactions.

To assess global changes in both the RBD and ligand structures during the triplicate MD runs, the root mean square deviation (RMSD) of the RBD alpha carbons and of the ligand, respectively, were analysed. Moreover, to evaluate the flexibility of the RBD with time, the root mean square fluctuation (RMSF) of the RBD side chains and alpha carbons was also observed (Fig. S19). In the RMSF plots, it was possible to observe a similar pattern across all three runs, in which the RBD terminals were the most flexible regions. This was expected, since these residues are typically connected to the rest of the spike protein. The initial binding pocket encompassed residues V44-L72, which is a comparatively rigid region of the RBD.

The Gibbs free energy variation of the system was also calculated over the course of the triplicate runs (Fig. S20), yielding total energy changes (Δ TOTAL) of -16.42 ± 5.23 , -19.23 ± 6.24 , and -18.14 ± 5.48 kcal/mol, respectively. The moving average remained below 0 kcal/mol and mostly below -10 kcal/mol, which is indicative of a very strong binding. The peaks observed in the third run at approximately

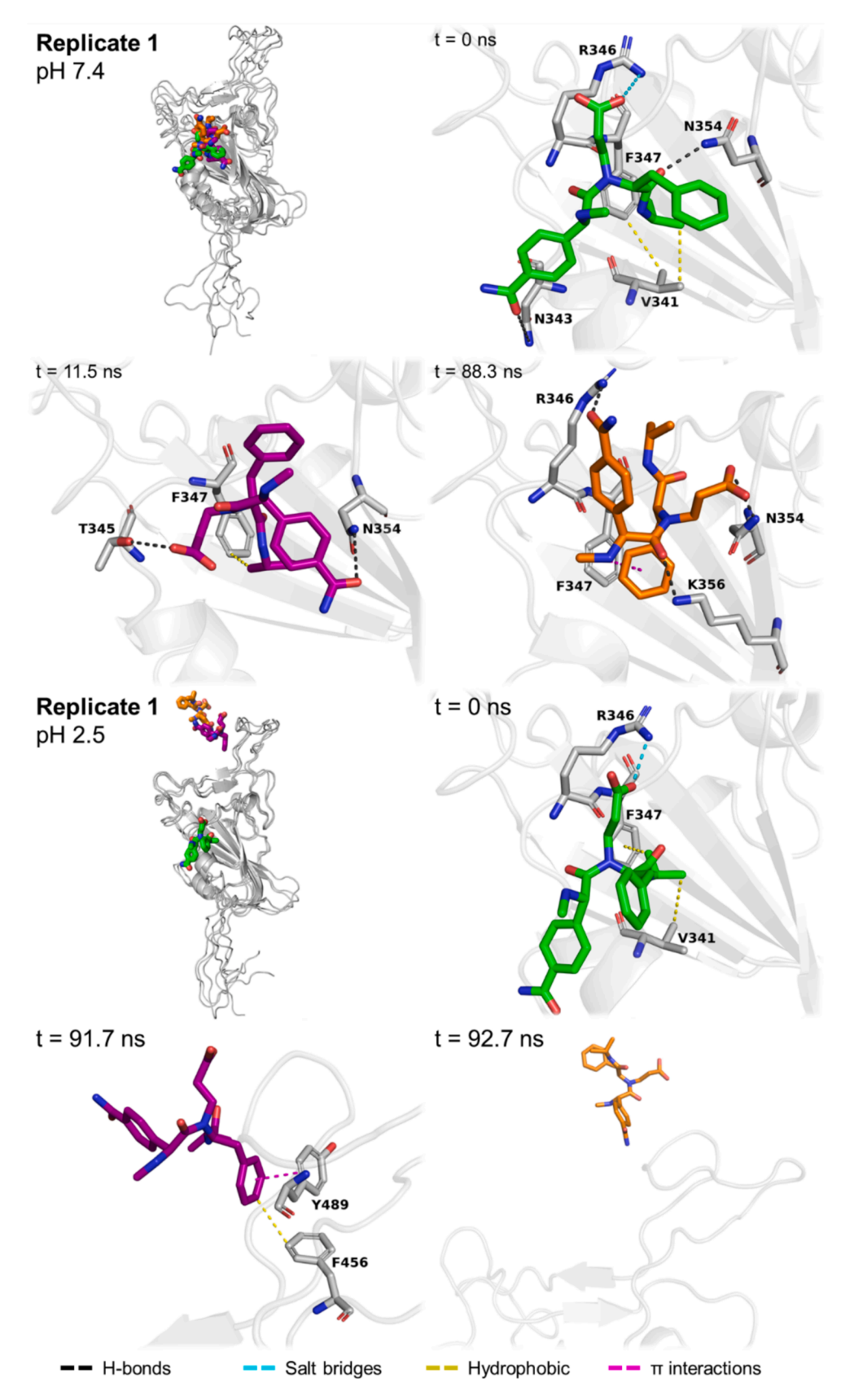


Fig. 6. Structural analysis of some of the main interactions during the first production run replicate of the RBD-lead ligand B1A3AL4 complex structure predicted by MOE under binding (pH 7.4) and elution conditions (pH 2.5). For better visibility, all hydrogens are hidden.

40–50 ns coincided with the migration of the ligand away from the initial binding pocket.

Next, the RBD and lead ligand structures were protonated to pH 2.5 using Open Babel and then submitted to triplicate MD runs to simulate elution conditions. The influence of pH on the disruption of important interactions was evident, as detachment of the ligand from the RBD occurred in all three runs (Fig. S6C). As the results were visualised in PyMOL (Fig. 6 and Figs. S21 and S22), it was evident the carboxylic acid of the ligand, its most active group under binding conditions, did not establish relevant or lasting interactions under elution conditions due to being protonated, and it led to the ligand detaching. Weaker interactions were observed, mainly hydrophobic, between the phenyl and isopropyl groups of the ligand and RBD hydrophobic residues.

The RMSD and RMSF were similarly calculated (Fig. S23). Although the global changes in the RBD and the ligand were negligible in the first and third runs, they were quite significant in the RBD in the second run starting at about 10 ns, before the detachment at 20 ns. The RMSF results were quite similar to those under binding conditions, indicating RBD flexibility is not affected by pH.

4. Conclusions

Based on the interactions established between the SARS-CoV-2 spike protein and known ligands, we designed a combinatorial library of 120 distinct small synthetic ligands, which were computationally and experimentally screened for binding to the spike protein. From this first library screening, 14 putative lead ligands were further evaluated for binding the target protein, after which five best performing ligands were further analysed, finally resulting in one lead adsorbent with the ligand B1A3AL4. With this adsorbent, we achieved > 95 % binding to spike proteins and 65-75 % recovery, maintaining its performance with an Omicron variant spike protein. When tested with a clarified supernatant sample, the spike protein enrichment factor was of 15, which can be useful in the context of a multi-step purification process. The key interactions between the spike protein RBD and the ligand were identified as mainly hydrophobic with some hydrogen bonds and the ligand carboxyl group establishing important electrostatic interactions. Finally, the process for the fast design and discovery of a synthetic ligand and respective adsorbent towards a specific antigenic viral target was herein successfully demonstrated, opening the possibility to apply to other targets of relevance in pandemics preparedness efforts.

It should be emphasized that the current manuscript focuses on ligand design and discovery, thus there are several aspects related to process development and optimization that should be considered as next steps, namely careful evaluation of HCP and DNA clearance, and testing with a wider range of crude samples containing spike protein variants and derived engineered versions. Another important aspect relates to the introduction of the proposed affinity capture step in a full purification process, in which other chromatographic and non-chromatographic unit operations are harmonized to reach a final desired high purity.

CRediT authorship contribution statement

Carlos Filipe Santos Costa: Methodology, Validation, Formal analysis, Investigation, Data curation, Writing – original draft. Iana Lychko: Methodology, Validation, Formal analysis, Investigation, Data curation. Carolina Mota Natal: Methodology, Validation, Formal analysis, Investigation, Data curation. Arménio Jorge Moura Barbosa: Methodology, Writing – review & editing, Supervision. Ana Margarida Gonçalves Carvalho Dias: Methodology, Writing – review & editing, Supervision. Ana Cecília Afonso Roque: Methodology, Resources, Writing – review & editing, Supervision, Funding acquisition.

Declaration of competing interest

The authors declare that they have no known competing financial

interests or personal relationships that could have appeared to influence the work reported in this paper.

Acknowledgements

This work was funded by the European Union's Horizon 2020 programme under grant agreement no. 899732 (PURE project); Fundação para a Ciência e a Tecnologia (FCT), I.P.; within the scope of the project UIDP/04378/2020 and UIDB/04378/2020 of UCIBIO; the project LA/P/0140/2020 of i4HB; project PROTEIOS - PTDC/CTM-CTM/3389/202; with support by INCD, 2023.10436.CPCA.A1 and 2023.10437.CPCA. A2, funded by FCT and FEDER under the project 01/SAICT/2016 no. 02215; the PhD scholarships 2020.07566.BD (CC) and 2023.01023.BD (CMN).

Appendix A. Supplementary material

Supplementary data to this article can be found online at https://doi.org/10.1016/j.seppur.2025.132778.

Data availability

Data will be made available on request.

References

- C. Maguire, et al., Molecular mimicry as a mechanism of viral immune evasion and autoimmunity, Nat. Commun. 15 (1) (2024) 9403, https://doi.org/10.1038/ s41467-024-53658-8
- [2] J. Zhang, et al., Virus-like structures for combination antigen protein mRNA vaccination, Nat. Nanotechnol. 19 (8) (2024) 1224–1233, https://doi.org/ 10.1038/s41565-024-01679-1.
- [3] C. Varanda, M.D.R. Félix, M.D. Campos, P. Materatski, An overview of the application of viruses to biotechnology, Viruses 13 (10) (2021) 2073, https://doi. org/10.3390/v13102073.
- [4] R. Castro, et al., Production of high-quality SARS-CoV-2 antigens: Impact of bioprocess and storage on glycosylation, biophysical attributes, and ELISA serologic tests performance, Biotechnol. Bioeng. 118 (6) (2021) 2202–2219, https://doi.org/10.1002/bit.27725.
- [5] N. Butani, Y. Xu, S. Pan, Y. Durocher, R. Ghosh, A fast, efficient, and scalable method for purifying recombinant SARS-CoV-2 spike protein, J. Chromatogr. B 1215 (2023) 123579, https://doi.org/10.1016/j.jchromb.2022.123579.
- [6] G. Salvatori, L. Luberto, M. Maffei, L. Aurisicchio, G. Roscilli, F. Palombo, E. Marra, SARS-CoV-2 SPIKE PROTEIN: an optimal immunological target for vaccines, J. Trans. Med. 18 (1) (2020) 222, https://doi.org/10.1186/s12967-020-02392-y.
- [7] A.M. Almehdi, G. Khoder, A.S. Alchakee, A.T. Alsayyid, N.H. Sarg, S.S.M. Soliman, SARS-CoV-2 spike protein: pathogenesis, vaccines, and potential therapies, Infection 49 (5) (2021) 855–876, https://doi.org/10.1007/s15010-021-01677-8.
- [8] R. Kumavath, et al., The spike of SARS-CoV-2: uniqueness and applications, Front. Immunol. 12 (2021) 663912, https://doi.org/10.3389/fimmu.2021.663912.
- [9] N. Cibelli, et al., Advances in purification of SARS-CoV-2 spike ectodomain protein using high-throughput screening and non-affinity methods, Scientif. Rep. (2021), https://doi.org/10.21203/rs.3.rs-778537/v1.
- [10] M.J.B. Matos, et al., A purification platform for antibodies and derived fragments using a *de novo* designed affinity adsorbent, Sep. Purif. Technol. 265 (2021) 118476, https://doi.org/10.1016/j.seppur.2021.118476.
- [11] R. dos Santos, C. Figueiredo, A.C. Viecinski, A.S. Pina, A.J.M. Barbosa, A.C. A. Roque, Designed affinity ligands to capture human serum albumin, J. Chromatogr. A 1583 (2019) 88–97, https://doi.org/10.1016/j.chroma.2018.11.021.
- [12] Í.L. Batalha, A.C.A. Roque, Petasis-Ugi ligands: New affinity tools for the enrichment of phosphorylated peptides, J. Chromatogr. B 1031 (2016) 86–93, https://doi.org/10.1016/j.jchromb.2016.07.035.
- [13] M. Cerff, A. Scholz, M. Franzreb, I.L. Batalha, A.C.A. Roque, C. Posten, In situ magnetic separation of antibody fragments from Escherichia coli in complex media, BMC Biotechnol. 13 (1) (2013) 1, https://doi.org/10.1186/1472-6750-13-44
- [14] T. Barroso, T. Casimiro, A.M. Ferraria, F. Mattioli, A. Aguiar-Ricardo, A.C. A. Roque, Hybrid monoliths for magnetically-driven protein separations, Adv. Funct. Mater. 24 (28) (2014) 4528–4541, https://doi.org/10.1002/ adfm.201400022.
- [15] T. Barroso, M. Temtem, A. Hussain, A. Aguiar-Ricardo, A.C.A. Roque, Preparation and characterization of a cellulose affinity membrane for human immunoglobulin G (IgG) purification, J. Membr. Sci. 348 (1) (2010) 224–230, https://doi.org/ 10.1016/j.memsci.2009.11.004.
- [16] A.S. Pina, Í.L. Batalha, A.M.G.C. Dias, A.C.A. Roque, Affinity Tags in Protein Purification and Peptide Enrichment: An Overview, in: N.E. Labrou (Ed.), Protein Downstream Processing: Design, Development, and Application of High and Low-

- Resolution Methods, Springer US, New York, NY, 2021, pp. 107–132, https://doi.org/10.1007/978-1-0716-0775-6 10.
- [17] C.S.M. Fernandes, et al., Retroviral particles are effectively purified on an affinity matrix containing peptides selected by phage-display, Biotechnol. J. 11 (12) (2016) 1513–1524, https://doi.org/10.1002/biot.201600025.
- [18] C.F.S. Costa, A.J.M. Barbosa, A.M.G.C. Dias, A.C.A. Roque, Native, engineered and de novo designed ligands targeting the SARS-CoV-2 spike protein, Biotechnol. Adv. 59 (2022) 107986, https://doi.org/10.1016/j.biotechadv.2022.107986.
- [19] F. Amanat, et al., A serological assay to detect SARS-CoV-2 seroconversion in humans, Nat. Med. 26 (7) (2020) 1033–1036, https://doi.org/10.1038/s41591-020-0013-5
- [20] The PyMOL Molecular Graphics System, Version 2.4.1. Schrödinger, LLC.
- [21] H.M. Berman, et al., The protein data bank, Nucleic Acids Res. 28 (1) (2000) 235–242, https://doi.org/10.1093/nar/28.1.235.
- [22] ChemSpider. Royal Society of Chemistry. [Online]. Available: http://www.chemspider.com/.
- [23] J. Eberhardt, D. Santos-Martins, A.F. Tillack, S. Forli, AutoDock Vina 1.2.0: new docking methods, expanded force field, and python bindings, J. Chem. Inf. Model. 61 (8) (2021) 3891–3898, https://doi.org/10.1021/acs.jcim.1c00203.
- [24] O. Trott, A.J. Olson, AutoDock Vina: improving the speed and accuracy of docking with a new scoring function, efficient optimization, and multithreading, J. Comput. Chem. 31 (2) (2010) 455–461, https://doi.org/10.1002/jcc.21334.
- [25] S. Dallakyan, A.J. Olson, Small-Molecule Library Screening by Docking with PyRx, in: J.E. Hempel, C.H. Williams, C.C. Hong (Eds.), Chemical Biology: Methods and Protocols, Springer, New York, NY, 2015, pp. 243–250, https://doi.org/10.1007/978.1.4939.2269-7
- [26] Molecular Operating Environment (MOE), 2022. Chemical Computing Group ULC, 910-1010 Sherbrooke St. W., Montreal, QC H3A 2R7.
- [27] E.F. Pettersen, et al., UCSF Chimera—a visualization system for exploratory research and analysis, J. Comput. Chem. 25 (13) (2004) 1605–1612, https://doi. org/10.1002/jcc.20084.
- [28] ChemDraw 20.1. Revvity Signals Software.
- [29] T. Sander, J. Freyss, M. von Korff, C. Rufener, DataWarrior: an open-source program for chemistry aware data visualization and analysis, J. Chem. Inf. Model. 55 (2) (2015) 460–473, https://doi.org/10.1021/ci500588j.
- [30] N.M. O'Boyle, M. Banck, C.A. James, C. Morley, T. Vandermeersch, G. R. Hutchison, Open Babel: an open chemical toolbox, J. Cheminform 3 (1) (2011) 1, https://doi.org/10.1186/1758-2946-3-33.
- [31] MarvinSketch 19.12. (2019). ChemAxon (http://www.chemaxon.com).
- [32] P. Steppert, et al., Purification of HIV-1 gag virus-like particles and separation of other extracellular particles, J. Chromatogr. A 1455 (2016) 93–101, https://doi. org/10.1016/j.chroma.2016.05.053.

- [33] M.J. Abraham, et al., GROMACS: High performance molecular simulations through multi-level parallelism from laptops to supercomputers, SoftwareX 1–2 (2015) 19–25, https://doi.org/10.1016/j.softx.2015.06.001.
- [34] K. Lindorff-Larsen, et al., 'Improved side-chain torsion potentials for the Amber ff99SB protein force field', Proteins: Struct. Function, Bioinformatics 78 (8) (2010) 1950–1958, https://doi.org/10.1002/prot.22711.
- [35] A.W. Sousa da Silva, W.F. Vranken, ACPYPE AnteChamber PYthon Parser interfacE, BMC Res. Notes 5 (1) (2012) 1, https://doi.org/10.1186/1756-0500-5-367.
- [36] J. Wang, W. Wang, P.A. Kollman, D.A. Case, Automatic atom type and bond type perception in molecular mechanical calculations, J. Mol. Graph. Model. 25 (2) (2006) 247–260, https://doi.org/10.1016/j.jmgm.2005.12.005.
- [37] J. Wang, R.M. Wolf, J.W. Caldwell, P.A. Kollman, D.A. Case, Development and testing of a general amber force field, J. Comput. Chem. 25 (9) (2004) 1157–1174, https://doi.org/10.1002/jcc.20035.
- [38] M.S. Valdés-Tresanco, M.E. Valdés-Tresanco, P.A. Valiente, E. Moreno, gmx_MMPBSA: a new tool to perform end-state free energy calculations with GROMACS, J. Chem. Theory Comput. 17 (10) (2021) 6281–6291, https://doi.org/10.1021/acs.ictc.1c00645.
- [39] B.R. Miller III, T.D. McGee Jr, J.M. Swails, N. Homeyer, H. Gohlke, A.E. Roitberg, MMPBSA. py: an efficient program for end-state free energy calculations, J. Chem. Theory Comput. 8 (9) (2012) 3314–3321, https://doi.org/10.1021/ct300418h.
- [40] OriginPro, Version 2021. OriginLab Corporation, Northampton, MA, USA.
- [41] S. Balkani, S. Shamekhi, R. Raoufinia, R. Parvan, J. Abdolalizadeh, Purification and characterization of bovine serum albumin using chromatographic method, Adv Pharm Bull 6 (4) (2016) 651–654, https://doi.org/10.15171/apb.2016.080.
- [42] T. Arakawa, K. Tsumoto, K. Nagase, D. Ejima, The effects of arginine on protein binding and elution in hydrophobic interaction and ion-exchange chromatography, Protein Expr. Purif. 54 (1) (2007) 110–116, https://doi.org/10.1016/j. pep.2007.02.010.
- [43] A. Hirano, K. Shiraki, T. Kameda, Effects of arginine on multimodal chromatography: experiments and simulations, CPPS 20 (1) (2018) 40–48, https://doi.org/10.2174/1389203718666171024115407.
- [44] Y. Li, The application of caprylic acid in downstream processing of monoclonal antibodies, Protein Expr. Purif. 153 (2019) 92–96, https://doi.org/10.1016/j. pep.2018.09.003.
- [45] D. Shukla, B.L. Trout, Understanding the role of arginine and citrate as eluents in affinity chromatography, in: Developments in Biotechnology and Bioprocessing, American Chemical Society, 2013, pp. 67–86, https://doi.org/10.1021/bk-2013-1125.ch005.
- [46] A. D'Arco, et al., Secondary Structures of MERS-CoV, SARS-CoV, and SARS-CoV-2 Spike Proteins Revealed by Infrared Vibrational Spectroscopy, Int. J. Mol. Sci. 24 (11) (2023) 11. https://doi.org/10.3390/ijms24119550.